Lifetimes of metal nanowires with broken axial symmetry

Lan Gong
Department of Physics, New York University, New York, New York 10003, USA

J. Bürki
Department of Physics and Astronomy, California State University Sacramento, Sacramento, California 95819-6041, USA

Charles A. Stafford
Department of Physics, University of Arizona, Tucson, Arizona 85721, USA

Daniel L. Stein
Department of Physics, New York University, New York, New York 10003, USA
and Courant Institute of Mathematical Sciences, New York University, New York, New York 10003, USA
(Received 7 October 2014; revised manuscript received 15 December 2014; published 5 January 2015)

We present a theoretical approach for understanding the stability of simple metal nanowires, in particular, monovalent metals such as the alkalis and noble metals. Their cross sections are of order 1 nm, so that small perturbations from external (usually thermal) noise can cause large geometrical deformations. The nanowire lifetime is defined as the time required for making a transition into a state with a different cross-sectional geometry. This can be a simple overall change in radius, or a change in the cross-section shape, or both. We develop a stochastic field theoretical model to describe this noise-induced transition process in which the initial and final states correspond to locally stable states on a potential surface derived by solving the Schrödinger equation for the electronic structure of the nanowire numerically. The numerical *string method* is implemented to determine the optimal transition path governing the lifetime. Using these results, we tabulate the lifetimes of sodium and gold nanowires for several different initial geometries.

DOI: 10.1103/PhysRevB.91.035401 PACS number(s): 05.40.−a, 62.23.Hj, 62.25.−g, 47.20.Dr

I. INTRODUCTION

Nanowires made of monovalent metals, such as sodium, copper, and gold, live at the boundary between classical and quantum mechanics and exhibit some of the behavior of each. They are therefore of great interest, from both a fundamental physics perspective as well as for technological applications. Their cross-sectional dimensions can be as small as half a nanometer (though several nanometers is far more typical) and their lengths at most a few tens of nanometers. At these length scales, the stresses induced by surface tension exceed Young's modulus, making the wires subject to deformation under plastic flow [1] and therefore subject to breakup due to the Rayleigh instability [2,3]. This in fact has been observed for copper nanowires annealed between 400 and 600 °C [4], as well as for copper and silver nanowires [5,6].

However, electron-shell filling effects stabilize these wires for radii near certain discrete "magic radii" [1]. These radii correspond to conductance "magic numbers" that agree with those measured in experiments [7–11]. This quantum stabilization, however, is only against small surface oscillations that can lead to breakup via the Rayleigh instability; it does not take into account thermal noise that can induce large radial fluctuations that can lead to breakup.

A self-consistent approach to determining lifetimes [12], which modeled thermal fluctuations through a stochastic Ginzburg-Landau classical field theory, obtained quantitative estimates of alkali nanowire lifetimes [12,13], in good agreement with experimentally inferred values [7,8]. The theory, however, is limited to wires with a cylindrical symmetry. Urban *et al.* [9,11], using a stability analysis of metal nanowires subject to nonaxisymmetric perturbations, showed that, at certain mean radii and aspect ratios, Jahn-Teller deformations breaking cylindrical symmetry can be energetically favorable, leading to an additional class of stable nanowires with *non*-axisymmetric cross sections.

The mathematical problem of determining nanowire lifetimes in this more general case requires solution of a stochastic set of coupled partial differential equations corresponding to a stochastic Ginzburg-Landau field theory with *two* coupled fields, one corresponding to variations in mean radius and the other to deviations from axial symmetry. In particular, we consider here quadrupolar deformations of the nanowire cross section, which cost less surface energy than higher-multipole deformations, and were shown to be the most common stable deformations within linear stability analyses [11,14]. The general mathematical treatment of such problems was discussed in [15,16]. Of particular interest was the discovery of a transition in activation behavior, not only as wire length varies [12], but also as bending coefficients for the two fields vary [16].

In this paper, we use these results and those of Urban *et al.* [9,11] to construct a more general theory of lifetimes of nanowires with both axisymmetric and nonaxisymmetric cross sections, as functions of temperature, strain, and other thermodynamic variables.

II. OVERVIEW OF THE NANOWIRE STABILITY PROBLEM

Historically, there have been a number of studies on nanowires focusing on aspects ranging from growth techniques

to electronic, mechanical, thermal, and optical properties. There are several major laboratory techniques for synthesizing nanowires: suspension, vapor-liquid-solid (VLS), solution-based growth, and so on. The materials used to fabricate nanowires also vary, including metals (e.g., Ni, Pt, Au), semiconductors (e.g., Si, InP, GaN, etc.), and insulators (e.g., SiO_2, TiO_2). Usually, the focus is on nanowires with cross sections of the order of hundreds of nanometers or even a few micrometers [17–19]. However, the type of nanowire under study here is much smaller—at most a few nanometers in radius [20]. The nanowires we study are mainly prepared via the suspension technique in either vacuum or air, as opposed to wires fabricated on a substrate and adhering to a surface.

Metal nanowires of atomic cross section are typically prepared using either a scanning tunneling microscope (STM) or a mechanically controllable break junction (MCBJ) [20]. In both cases, the nanowires are essentially freely suspended three-dimensional wires. In the STM setup, a nanowire is obtained by pushing the sharp STM tip into a substrate and then carefully retracting it in a controlled way. The contact formed in this way is of atomic dimensions [21]. If the tip is moved further away, the contact thins down and eventually breaks. In the MCBJ method [22,23], the sample is fixed onto an insulating substrate and then bent by a piezoelectric drive controlled by an applied voltage. The sample is pulled apart until the wire breaks, after which it reforms by reversing the process. The displacement between the electrodes can be controlled with accuracy down to 100 fm. Because this setup is more stable against external vibration than the STM method, it allows more precise experiments on individual contacts. In both methods, the cross-sectional area of the nanowire is inferred from conductance measurements using the corrected Sharvin formula [11],

$$\frac{G_s}{G_0} = \frac{k_F^2 \mathcal{A}}{4\pi} - \frac{k_F \mathcal{P}}{4\pi} + \frac{1}{6}, \tag{1}$$

which gives an approximation G_s to the quantized conductance of an ideal metal nanowire in terms of geometrical quantities, such as the wire's minimal cross-sectional area $\mathcal{A}$ and corresponding cross-section perimeter $\mathcal{P}$. Here $G_0 = \frac{2e^2}{h}$ is the quantum of conductance and k_F is the Fermi wave vector of the material.

The formation and breakup process is repeated thousands of times to derive a statistical histogram for the conductance [7,24,25] (and therefore cross-sectional areas). The experiments can be performed at either ambient or cryogenic temperatures. Very small contacts consisting of four gold atoms in a row have been formed by means of this technique [26]. Although this type of experiment does not measure lifetimes of nanowires directly, rough estimates can be inferred from the existence of a conductance peak (which is evidence of a more stable wire, see Ref. [14]) by knowing parameters of the experiment's dynamics, in particular, the speed of elongation of the wire. Typically, the existence of a conductance peak in a MCBJ experiment [7] implies a nanowire lifetime greater than 1 ms.

Based on these criteria, there is ample experimental evidence that nanowires made from sodium, gold, and aluminum are stable, with lifetimes greater than or of the order of milliseconds [10,11,14].

From a theoretical point of view, the stability of metal nanowires can be explained by quantum-size effects, or electron-shell effects, that can overcome the classical Rayleigh instability [2] in very thin wires. While the Rayleigh instability makes thin wires unstable once their surface tension exceeds their yield strength [27], shell effects can stabilize wires with certain preferred cross sections. The nanowire is a quantum system where conduction electrons are confined within the surface of the wire, with a Fermi wavelength comparable to the cross-section linear dimension. This leads to electron-shell filling [28–30], which provides an oscillating potential with multiple minima as a function of the cross-section size and

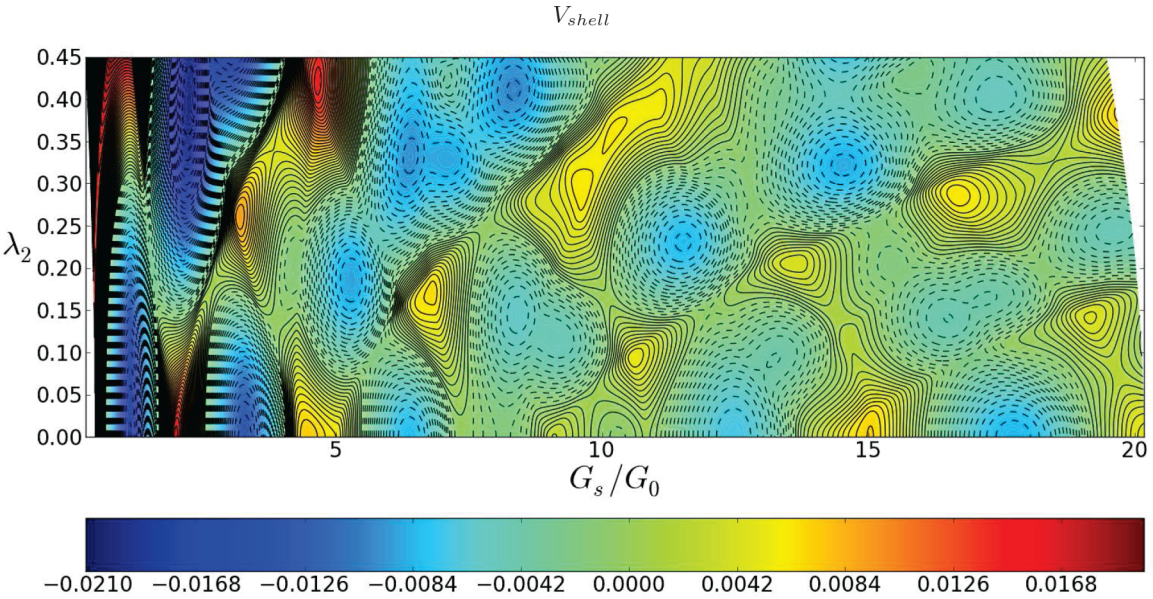

FIG. 1. (Color online) Contour plot of the electron-shell potential V_{shell} as a function of the Sharvin conductance G_s, defined by Eq. (1), and the quadrupolar deformation parameter λ_2.

shape. This potential is called the *electron-shell potential*, and its derivation is discussed in detail in Sec. III. Figure 1 shows this shell potential for wires with a quadrupolar cross section as a function of the wire's Sharvin conductance G_s [related to the cross-section area through Eq. (1)] and parameter λ_2, which describes the cross-section's deviation from a disk (with $\lambda_2 = 0$).

Quantum effects can thus stabilize the wire against breakup due to the Rayleigh instability. A linear stability analysis [11,31,32] shows that cylindrical wires are most stable when the radius of the cross section takes a series of discrete values called the "magic radii." It also finds that some wires with nonaxisymmetric cross sections can be stabilized by electron-shell effects. In fact, comparison of the sequence of stable structures observed in experiments with linear stability analyses implies that some of the experimentally observed conductance peaks must correspond to wires with nonaxisymmetric cross sections [10,14].

However, linear stability analyses typically consider only stability toward small, long-wavelength deformations of the wire. (See Refs. [32,33] for a linear analysis, including short-wavelength deformations.) In particular, they do not consider changes of radius or breakup due to large fluctuations, which can be initiated by thermal noise, application of stress, or other destabilizing effects. Because the regions of stability are confined by finite energy barriers (as can be seen from Fig. 1), a given structure is at best metastable; its confining barriers can be surmounted by thermal (or other) noise.

The energy contours shown in Fig. 1 lead naturally to a description of the lifetime problem in which (meta)stable structures correspond to local energy minima; in the limit of low noise (thermal energy small compared to the lowest confining barrier), there is an *optimal transition path* along which the probability of a successful transition is maximized [34]. When the zero-noise dynamics are governed by a potential function (as is the case here), the "barrier" corresponds to a saddle point in the potential surface, that is, a fixed point whose linearized dynamics has a single unstable direction, all the others being stable. The transition rate is governed by Kramers' formula

$$\Gamma \sim \Gamma_0 \exp(-\Delta E/k_B T), \tag{2}$$

where ΔE is the difference in energy between the saddle and the initial state and Γ_0 is a prefactor depending on the fluctuations around each. In the low-noise limit, the lifetime of a metastable state is just the inverse of the Kramers' transition rate. The problem then reduces to finding ΔE and Γ_0 as a function of the system parameters.

In the limit of weak noise, Wentzell and Freidlin (WF) [35] showed that a rigorous asymptotic estimate for the rate of transition (i.e., probability of a successful transition per unit time) can be found by constructing an *action functional*, which gives the relative probabilities of different paths. It has been shown for gradient systems [36,37] that the optimal transition path is one in which the system climbs uphill against the gradient through a saddle state and then relaxes toward its final state.

Solving for the transition rate therefore requires knowledge of the saddle state. The model developed in Ref. [15] allows for an analytical solution to the saddle state in the case of certain special potentials. To solve the nanowire stability problem, however, we need to find the transition path and lifetime in more general cases. The *string method* [38,39] is a numerical scheme designed for this kind of problem. The procedure it uses is to first guess the optimal path and then let it evolve freely along the direction of steepest descent until equilibrium is reached. Details of the application of the string method to the kind of problem discussed here are given in Ref. [16].

In the case of cylindrical wires, the cross section of the wire can in principle shrink or grow under the influence of noise. However, nanowires studied in experiments are typically suspended between two electrodes that apply a strain on the wire that tends to pull it apart; as a consequence, transitions are biased toward smaller radii. In either case, the electrodes act as a "particle bath" that can supply or remove atoms from the wire.

The case of transitions between different radii under the assumption of constant axisymmetry was studied in Ref. [12]. This corresponds to transitions between energy minima along the $\lambda_2 = 0$ axis in Fig. 1, and the calculated lifetimes of cylindrical nanowires are comparable with experimental values. Here we include the effects of broken axial symmetry, so that transitions between any two minima in Fig. 1 can occur in principle.

The space of possible transitions is large. However, the study can be narrowed to those of greatest physical significance, guided by linear stability analyses [9,11] and experiments on alkali metal nanowires [7,8,10]. In particular, nanowires with electrical conductance $G/G_0 = 5,9$, and 29, where $G_0 = 2e^2/h$ is the conductance quantum, were identified as the most stable nanowire structures with broken axial symmetry. We therefore concentrate on transitions from these local minima.

We will denote nonaxisymmetric structures by D (for deformed) and the cylindrical ones by C. So, for example, the nonaxisymmetric structure with $G/G_0 = 5$ will be denoted $D5$, the cylindrical structure with $G/G_0 = 3$ will be denoted $C3$, and so on.

III. THE MODEL

Metal nanowires have two main components which require different treatments. Conduction electrons have a wavelength at the Fermi surface that is of the order of the linear dimension of the wire cross section, and must therefore be treated quantum mechanically [29], and positive ions which are much heavier and therefore have much shorter wavelengths. As a result, the ions can be treated classically [27] and have a dynamics that is slow compared to that of the electrons, which can be treated separately [3]. This separation of time scales allows for a Born-Oppenheimer approximation, where conduction electrons are considered at all times to be in equilibrium with the instantaneous ionic structure which confines them within the wire. Furthermore, for wires in the size regime dominated by electron-shell effects, the discrete atomic structure is unimportant and can be replaced by a continuum of positive charge (the Jellium model [3,29,40]). Electron shell effects are dominant over atomic shell effects in small wires (at least up to about $40\,G_0$ for alkali metal [10] and Al wires [14], and are still present above that limit).

These observations form the basis for the nanoscale free-electron model (NFEM [11,29,41]) which considers electrons

in the wire to be free (other than being confined within the wire) and noninteracting. The former works best for s-shell metals, such as alkali and to some extent noble metals like gold, but has also been shown to perform well for metals whose Fermi surface in the extended zone scheme is nearly spherical, such as Al [14]. The limitation to noninteracting electrons has been shown to be a reasonable approximation for most metal nanowires [42].

A. Energetics of the nanowire

The surface of a nanowire aligned along the z axis can be described by a generalized radius function $R(z,\theta)$ in cylindrical coordinates, which can be written as a multipole expansion

$$R(z,\theta) = \rho(z)\left(\sqrt{1-\sum_m \lambda_m(z)^2/2} + \sum_m \lambda_m(z)\cos[m(\theta-\theta_m(z))]\right), \quad (3)$$

where the sums run over the positive integers. $\rho(z)$ defines the mean radius at position z along the wire, $\lambda_m(z)$ describes a multipolar deformation of order m, and $\theta_m(z)$ allows for a "twisting" of the wire cross section along z, which has no effect on the wire energy given the use of the adiabatic approximation (see below), and will therefore be dropped. The square root in Eq. (3) has been chosen so that the cross-section area $\mathcal{A} = \pi\rho^2(z)$.

Urban *et al.* [9,11] have shown that, aside from axisymmetric wires, by far the most common stable nanowires are wires with a quadrupolar cross section ($m = 2$). This is related to the fact that the surface-energy cost of deformations is proportional to m^2. Note that $m = 1$ deformations correspond to a simple translation combined with higher-order deformations. For that reason, we will restrict ourselves to quadrupolar deformations with $m = 2$, so that the shape of the wire will be described by two parameters: the mean radius $\rho(z)$ and the cross-section deformation parameter $\lambda_2(z)$, which correspond to the shape shown in Fig. 2.

As long as the variation of the wire cross section along z is slow enough (adiabatic approximation), any thermodynamic quantity can be written as an integral over z of a local quantity that depends only on the cross section at z. This is particularly true [29] for the grand-canonical potential Ω_e of the conduction electrons, which is the appropriate thermodynamic potential

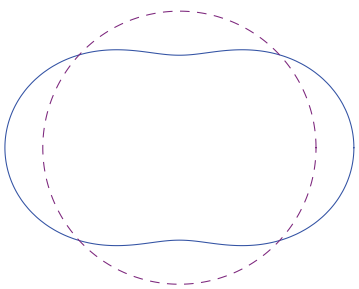

FIG. 2. (Color online) Cross section (solid line) of a nanowire with a quadrupolar deformation ($m = 2$).

for electrons in a wire connected to bulk electrodes (open system). Ω_e can thus be calculated for any wire of length L as a functional of $\rho(z)$ and $\lambda_2(z)$:

$$\Omega_e[T;\rho(z),\lambda_2(z)] = \int_0^L dz\,\omega[T,\rho(z),\lambda_2(z)], \quad (4)$$

where the local energy density $\omega(T,z)$ can be obtained numerically from the transverse energy levels $E_n[\rho(z),\lambda_2(z)]$ using the WKB approximation. The energy levels themselves can be calculated numerically for any value of λ_2 and depend on ρ in a simple way [11,29].

On the other hand, any extensive thermodynamic quantity can be expressed in terms of a Weyl expansion [43],

$$\Omega_e[\rho,\lambda_2] = -\omega\mathcal{V} + \sigma_s\mathcal{S} + \int_0^L V_{\text{shell}}[\rho,\lambda_2]\,dz, \quad (5)$$

where $\mathcal{V}$ and $\mathcal{S}$ are the wire's volume and surface area, respectively. The last term is a quantum correction and can be taken as the definition of the electron-shell potential V_{shell}, depicted in Fig. 1.

In the spirit of the Born-Oppenheimer approximation, the electronic grand canonical potential Ω_e is treated as the potential energy of the ions. Since the wire can also exchange ions with the bulk electrodes, the appropriate free energy determining the structure of the wire is the ionic grand canonical potential

$$\Omega_a[\rho,\lambda_m] = \Omega_e[\rho,\lambda_m] - \mu_a\mathcal{N}_a, \quad (6)$$

where μ_a is the chemical potential [3,12] of the ions determined by the electrodes, and $\mathcal{N}_a$ is the number of ions in the wire.

B. Effective energy of deformations

While linear stability is a necessary condition for a nanostructure to be observed experimentally, it is not sufficient due to large stochastic deviations, which can bring the wire out of its linearly stable state. Under the framework of the NFEM, we study the noise-induced fluctuations of the cross section by introducing two classical fields as perturbations to the parameters $\bar\rho$ and $\bar\lambda_2$ of the generalized radius function in Eq. (3):

$$\begin{aligned}\rho(z) &= \bar\rho\,(1+\phi_1(z)),\\ \lambda_2(z) &= \bar\lambda_2 + \phi_2(z),\end{aligned} \quad (7)$$

where $(\bar\rho,\bar\lambda_2)$ is the location of the local minimum of the ionic grand canonical potential.

Expanding the ionic grand canonical potential (6) around $(\bar\rho,\bar\lambda_2)$ with respect to the fields ϕ_1, ϕ_2, and keeping terms up to quadratic order in the spatial derivatives, we get the fluctuation energy functional. The ionic grand canonical potential (6) becomes

$$\begin{aligned}\Omega_a[\rho,\lambda_2] &= \Omega_a[\bar\rho\,(1+\phi_1),\bar\lambda_2+\phi_2]\\ &= L\left\{\pi\sigma_s\bar\rho\,f[\bar\lambda_2] + \left(1-\frac{\bar\rho}{2}\partial_{\bar\rho}\right)V_{\text{shell}}[\bar\rho,\bar\lambda_2]\right\}\\ &\quad + \int_{-L/2}^{L/2}\mathcal{H}[\phi_1(z),\phi_2(z)]\,dz,\end{aligned} \quad (8)$$

where $2\pi\bar\rho f$ is the perimeter of the metastable nanowire's cross section, and f may be represented by a quartic

polynomial with high accuracy:

$$f[\lambda_2] = 1 + \frac{3\lambda_2^2}{4} - \frac{9\lambda_2^4}{32}. \tag{9}$$

$\mathcal{H}$ is the energy density of fluctuations at position z,

$$\begin{aligned}\mathcal{H}[\phi_1(z),\phi_2(z)] = \frac{1}{2}\pi\sigma_s\bar{\sigma}^3\Bigg(&\left\{2 - \frac{\bar{\lambda}_2^2}{2} + \frac{71\bar{\lambda}_2^4}{16}\right\}(\phi_1')^2 \\ &+ 2\bar{\lambda}_2\left\{1 + \frac{\bar{\lambda}_2^2}{4}\right\}\phi_1'\phi_2' + \left\{1 - \frac{5\bar{\lambda}_2^2}{4}\right\}(\phi_2')^2\Bigg) \\ &+ U[\phi_1(z),\phi_2(z)]\end{aligned} \tag{10}$$

with the effective potential

$$\begin{aligned}U[\phi_1(z),\phi_2(z)] = &-\bar{\rho}\,\partial_{\bar{\rho}}V_{\text{shell}}[\bar{\rho},\bar{\lambda}_2]\phi_1 + 2\pi\sigma_s\bar{\rho}\,f'[\bar{\lambda}_2]\phi_2 \\ &- \bar{\rho}\left(\pi\sigma_s f[\bar{\lambda}_2] + \frac{1}{2}\partial_{\bar{\rho}}V_{\text{shell}}[\bar{\rho},\bar{\lambda}_2]\right)\phi_1^2 \\ &+ 2\pi\sigma_s\bar{\rho}\,f'[\bar{\lambda}_2]\phi_1\phi_2 + \pi\sigma_s\bar{\rho}f''[\bar{\lambda}_2]\phi_2^2 \\ &+ V_{\text{shell}}[\bar{\rho}(1+\phi_1),\bar{\lambda}_2+\phi_2] - V_{\text{shell}}[\bar{\rho},\bar{\lambda}_2].\end{aligned} \tag{11}$$

Here σ_s is the material-dependent surface tension: for gold $\sigma_s = 7.83\,(\text{eV/nm}^2)$; for sodium $\sigma_s = 1.39\,(\text{eV/nm}^2)$. L is the length of the wire. The electron-shell potential V_{shell} has to be obtained separately from solving for the electronic energy bands in the transverse direction numerically [11].

C. The dynamical system

As discussed in Refs. [15,16], the time evolution of the fields under noise can be described by the coupled Langevin equations

$$\dot{\vec{\Phi}} = -\frac{\delta H[\vec{\Phi}]}{\delta\vec{\Phi}} + \sqrt{2\epsilon}\,\vec{\xi}(z,t),$$

where $\vec{\Phi} = \binom{\phi_1}{\phi_2}$ and $\vec{\xi}(z,t)$ is Gaussian spatiotemporal white noise with $\epsilon = k_B T$. The saddle state is an extremum of the action $H[\vec{\Phi}]$ [34], and so the optimal transition path can be obtained numerically by evolving $\vec{\Phi}$ according to the noise-free form of the dynamical equations above.

For convenience, we make a change of variable $\phi_1,\phi_2 \to \psi_1,\psi_2$ to eliminate the cross term $\phi_1'\phi_2'$ in Eq. (10). The two new fields are defined as

$$\psi_1 = \phi_1 + \frac{g_{12}}{g_1}\phi_2, \quad \psi_2 = \phi_2, \tag{12}$$

with

$$g_1 = \pi\sigma_s\bar{\rho}^3\left(2 - \frac{\bar{\lambda}_2^2}{2} + \frac{71\bar{\lambda}_2^4}{16}\right), \quad g_{12} = \pi\sigma_s\bar{\rho}^3\bar{\lambda}_2\left(1 + \frac{\bar{\lambda}_2^2}{4}\right), \quad g_2 = \pi\sigma_s\bar{\rho}^3\left(1 - \frac{5\bar{\lambda}_2^2}{4}\right). \tag{13}$$

The resulting equations of motion for ψ_1 and ψ_2 are

$$\begin{aligned}\dot{\psi}_1 = {}& g_1\psi_1'' + \bar{\rho}(\partial_{\bar{\rho}}V_{\text{shell}}[\bar{\rho},\bar{\lambda}_2]) + 2\bar{\rho}\left(\pi\sigma_s f[\bar{\lambda}_2] + \frac{1}{2}\partial_{\bar{\rho}}V_{\text{shell}}[\bar{\rho},\bar{\lambda}_2]\right)\psi_1 \\ &- \left[2\pi\sigma_s\bar{\rho}\,f'[\bar{\lambda}_2] + 2\bar{\rho}\left(\pi\sigma_s f[\bar{\lambda}_2] + \frac{1}{2}\partial_{\bar{\rho}}V_{\text{shell}}[\bar{\rho},\bar{\lambda}_2]\right)\frac{g_{12}}{g_1}\right]\psi_2 - \bar{\rho}\,\partial_\rho V_{\text{shell}}[\rho,\lambda_2], \\ \dot{\psi}_2 = {}& \left(g_2 - \frac{g_{12}^2}{g_1}\right)\psi_2'' - \left(2\pi\sigma_s\bar{\rho}\,f'[\bar{\lambda}_2] + \bar{\rho}\,\partial_{\bar{\rho}}V_{\text{shell}}[\bar{\rho},\bar{\lambda}_2]\frac{g_{12}}{g_1}\right) \\ &+ \left[2\bar{\rho}\left(\pi\sigma_s f[\bar{\lambda}_2] + \frac{1}{2}\partial_{\bar{\rho}}V_{\text{shell}}[\bar{\rho},\bar{\lambda}_2]\right)\frac{g_{12}^2}{g_1^2} + \pi\sigma_s\bar{\rho}\,f'[\bar{\lambda}_2]\frac{g_{12}}{g_1} - 2\pi\sigma_s\bar{\rho}f''[\bar{\lambda}_2]\right]\psi_2 \\ &- \left[2\pi\sigma_s\bar{\rho}\,f'[\bar{\lambda}_2] + 2\bar{\rho}\left(\pi\sigma_s f[\bar{\lambda}_2] + \frac{1}{2}\partial_{\bar{\rho}}V_{\text{shell}}[\bar{\rho},\bar{\lambda}_2]\right)\frac{g_{12}}{g_1}\right]\psi_1 + \frac{g_{12}}{g_1}\bar{\rho}\,\partial_\rho V_{\text{shell}}[\rho,\lambda_2] - \partial_{\lambda_2}V_{\text{shell}}[\rho,\lambda_2],\end{aligned} \tag{14}$$

where $\dot{\psi} = \partial\psi/\partial t$ and $\psi' = \partial\psi/\partial z$. We now turn to the solution of the optimal transition path using the string method.

IV. RESULTS

In Ref. [16] the string method was applied to the problem of noise-induced transitions in a two-component classical field theory. The transition path, or *string*, starts in a random configuration on the potential surface, with its two ends inside the basins of attraction of the initial and final states, respectively. The string is then allowed to evolve along the direction of the energy gradient, thereby determining the optimal transition path. The saddle state is the configuration of highest energy along this path. The results were consistent with the analytical solutions of [15], in particular, the transition of the saddle state from a homogeneous to an instanton configuration as L increases beyond a critical value L_c.

In the following, we apply the same numerical scheme to the ionic grand canonical potential surface of a metal nanowire, in order to study lifetimes of wires whose cross sections correspond to the conductance plateaus $D5$ and $D9$.

It was found theoretically in Ref. [12] that both the activation barriers and the transition direction are sensitive to changes in stress of the order of 1nN. Figure 3 shows the activation barrier for the transition of a cylindrical gold

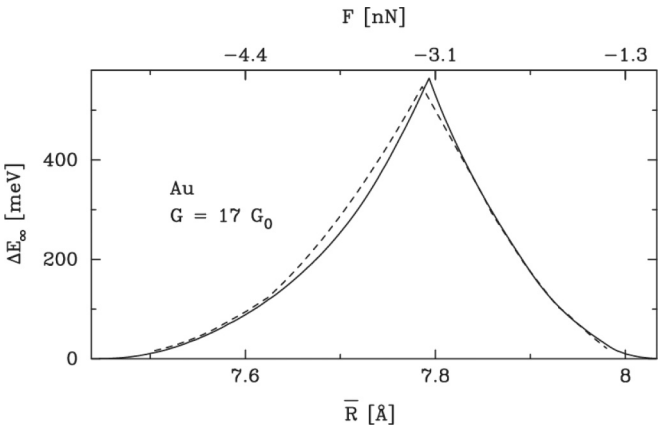

FIG. 3. The activation barrier ΔE_∞ as a function of mean radius for the conductance plateau $G_s/G_0 = 17$ of gold. Solid curve: numerical result for the full potential; dashed curve: result from theoretical calculation [12] using the best cubic-polynomial fit to the full potential. The mean radius is related to the tensile stress (upper axis). This figure is taken from Ref. [12].

nanowire on the conductance plateau $G/G_0 = 17$ (denoted $C17$) to other linearly stable structures. To the left of the cusp, the transition proceeds in a direction corresponding to thinning (equivalently, moving to a lower conductance value); to the right, the transition proceeds via thickening (moving to a higher conductance value). The most stable structure of $C17$ corresponds to the maximum value of ΔE_∞, which is located at the cusp; at this point the activation barriers for thinning and growth are equal.

For a nonaxisymmetric wire, by contrast, it is unlikely for thinning and growth processes to reach equilibrium at the same stress; the cusp in Fig. 3 is therefore absent. The greater richness of the configuration space for nonaxisymmetric wires allows more options for escape from a given initial state; barriers are therefore generally lower (and lifetimes shorter) than in situations restricted to axial symmetry.

Detailed analysis shows that there are two types of instanton transition states that may arise as the initial state of the wire varies. The first corresponds to decay into the nearest cylindrical structure and resembles an asymmetric hyperbolic tangent function with the longer arm coinciding with the initial configuration (see Fig. 4). The second corresponds to decay into (usually) the second-nearest-neighbor cylindrical structure, and consists of multiple plateaus, each corresponding to a local minimum the transition goes through (see Fig. 5). We hereafter refer to the first as a "short instanton" and the second as a "long instanton." The final state of the latter is farther from the initial state in configuration space than that of the former.

Switching between short and long instantons is caused by the change in the behavior of the activation barrier as a function of L. Within a given family of wires (e.g., $D5$) lying in a particular basin of attraction of the electron-shell potential, there is a qualitative difference in the activation behavior of the thinner wires versus the thicker wires, which can be tuned by applying tensile/compressive stress. For thinner wires (e.g., under tensile stress), the energy of the short instanton first grows for $L < L_c$ and then reaches a plateau for $L > L_c$; for thicker wires (e.g., under compression), it continues growing as L increases beyond L_c. The upper bound of the lifetime for the transition consequently grows without bound in the

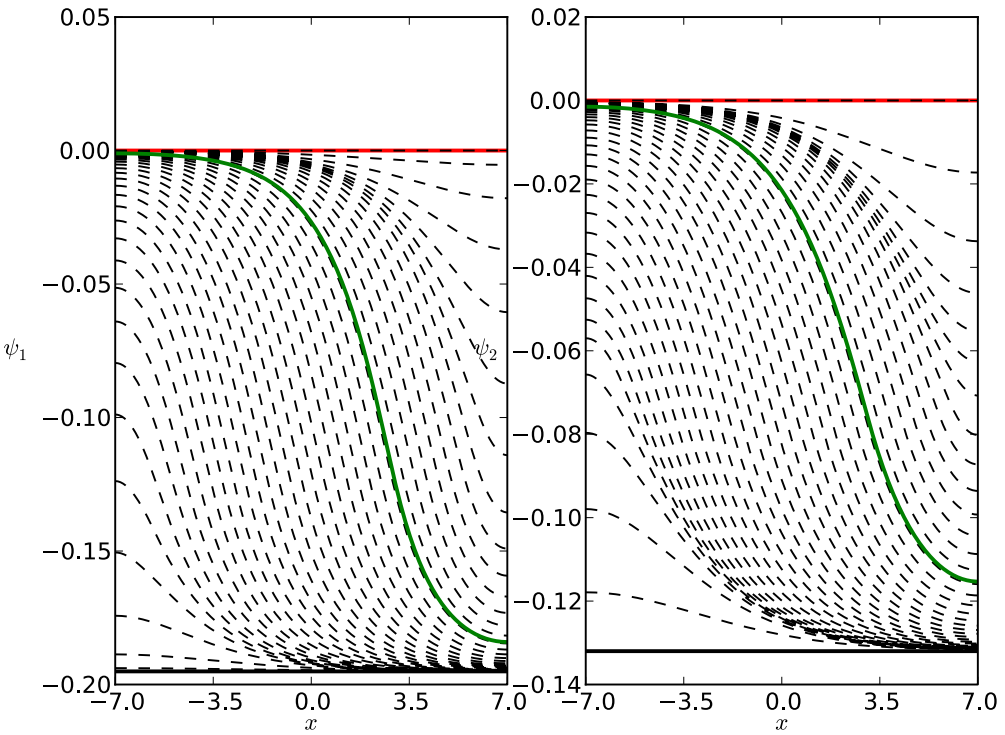

FIG. 4. (Color online) A typical configuration of the short instanton (green), where the transition starts from the initial $D5$ configuration at $G_s/G_0 = 5.55$ (red line) and ends at its nearest-neighbor state $C3$ (thick black). Here a gold wire of length 1.2 nm is considered. The dashed black lines are other intermediate states along the transition path.

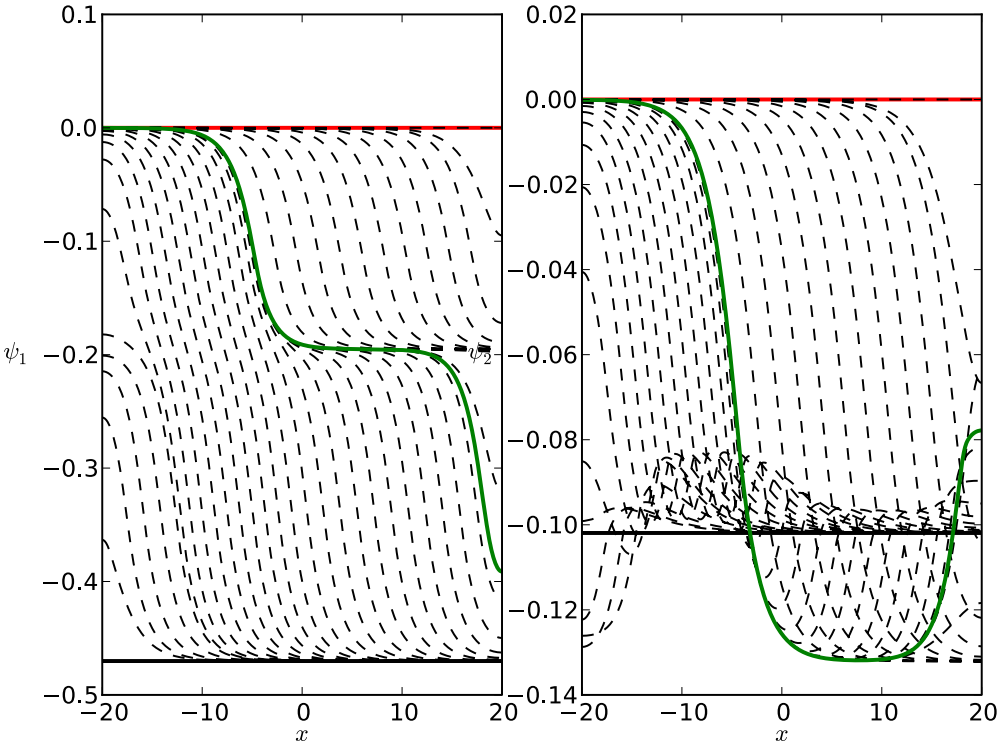

FIG. 5. (Color online) A typical configuration of the long instanton, where the transition starts from the initial $D5$ configuration at $G_s/G_0 = 5.56$ and ends at its second-nearest-neighbor state $C1$. Note that there are two obvious plateaus in the shape of the long instanton, with one corresponding to the initial state and the other to the intermediate local minimum $C3$. Here a gold wire of length 3.3 nm is considered. The line styles follow the same convention as in Fig. 4.

latter case as L increases. Conversely, the energy of the long instanton approaches a finite asymptotic value as $L \to \infty$. Therefore, for thicker wires in a given family, the energies of the short and long instanton cross at a certain L, beyond which the short instanton transition state is no longer favorable (see Fig. 6).

The change in the energy behavior of the short instanton can be understood by modeling the transition using an asymmetric double-well potential. In such a system [shown in Fig. 7(a)], the activation barrier of the state belonging to the upper well is finite and independent of L as $L \to \infty$; consequently, the leading-order exponential term determining the lifetime [Eq. (2)] approaches a constant value. In the other direction, however, the lifetime of the lower well, as determined by its transition rate to the upper one [shown in Fig. 7(b)], is not bounded because the activation barrier grows with L: $\Delta E \sim C \cdot L$, with C a constant determined by the energy difference between the two wells. When the cross section of the wire is varied by adjusting the applied tensile force, the two potential wells (representing the two linearly stable states) shift vertically relative to one another, until the lower well becomes the new upper well and vice versa.

Consider now the thinning process for wires under tension; as an example, we study the situation where the state $D5$ corresponds to the upper well and $C3$ to the lower well. Under tension, the activation barrier ΔE_∞, and hence the lifetime of the thinning process from $D5 \to C3$, is always bounded. Under compression, however, $D5$ shifts downward to become the lower well and $C3$ the upper; now ΔE_∞ and the corresponding lifetime become unbounded as $L \to \infty$.

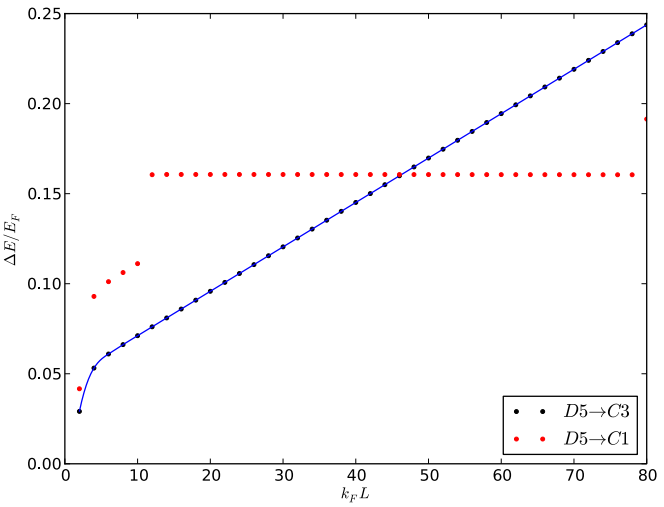

FIG. 6. (Color online) Activation barrier for thinning of the sodium $D5$ state, where the initial structure has $G_s/G_0 = 5.52$. There are two different final states: $C3$ and $C1$, to which the transition is via the short ($C3$) and long instanton ($C1$), respectively. The x axis is in dimensionless units whose range corresponds to 0–8.8 nm. Note that there is a discontinuity in the barrier of the transition $D5 \to C1$, below which it suddenly drops and becomes inclined. For very short wires, the long instanton is not favorable and "collapses" into two short instantons, where the first is the saddle state of the transition $D5 \to C3$ and the second is the saddle state of the transition $C3 \to C1$. The string method can only select the saddle of the highest energy if there is more than one along the transition path; here it is that of $C3 \to C1$, so that the activation barrier calculated increases with L.

The switch from short-instanton to long-instanton

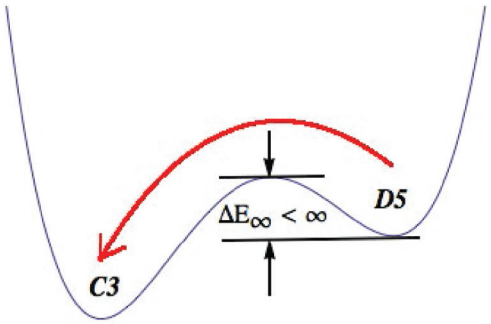

(a) Forward transition via short-instanton

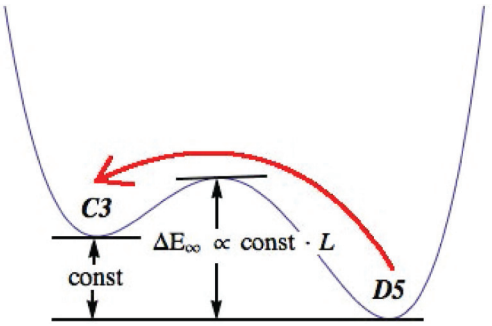

(b) Backward transition via short-instanton

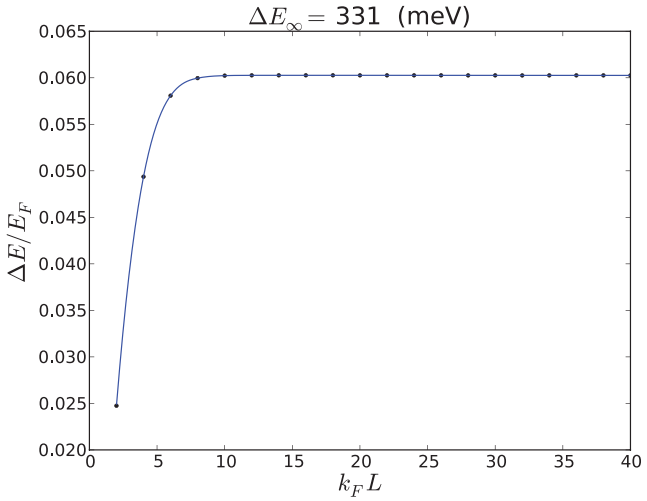

(c) Barrier of forward transition

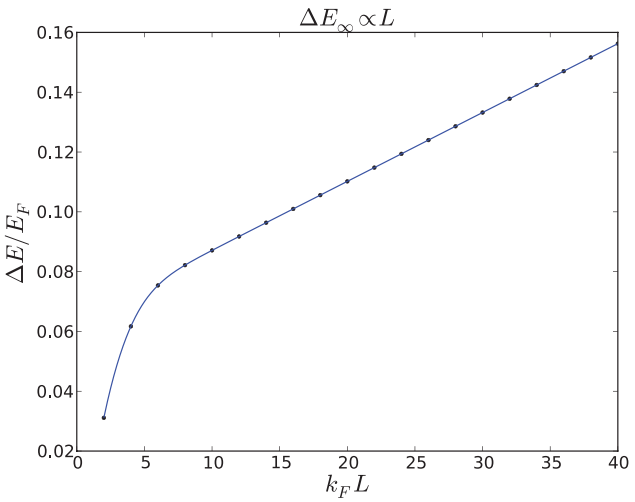

(d) Barrier of backward transition

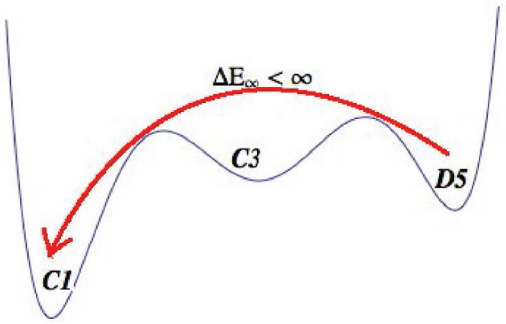

(e) The onset of long instanton

FIG. 7. (Color online) The first four subplots show the transition and the activation barrier of the $D5 \to C3$ transition for Au via the short instanton. Two different situations are shown: under tension at $G_s/G_0 = 5.5$ [Figs. 7(a) and 7(c)] the activation behavior displays the characteristics of the forward transition, while under compression at $G_s/G_0 = 5.6$ [Figs. 7(b) and 7(d)] the activation behavior displays the characteristics of the backward transition. The activation barrier of the forward transition levels out as $L \to \infty$, while that of the backward transition grows almost linearly with L, following the discussion of the asymmetric double-well model. The greater the difference in energy between the two metastable states, the faster ΔE grows with L. The last subplot sketches the transition from $D5$ to $C1$ via the long instanton, which sets a bound [as shown in Fig. (6)] on the barrier for thinning of $D5$ when the transition to $C3$ is backward.

The implication from this asymmetric double-well model is that, to have a bounded lifetime, it is necessary to find a final state whose energy is lower than that of $D5$. $C1$ is such a state; the lifetime of $D5 \to C1$ is bounded while that of $D5 \to C3$ is not. These results are summarized in Fig. 7.

We can infer some of the dynamics of the process of escape from the shape of the long instanton. Figure 5 implies that during the escape process part of the wire assumes the $C3$ state, which then bends further towards $C1$. We do not expect the long instanton to be a relevant intermediate state for escape

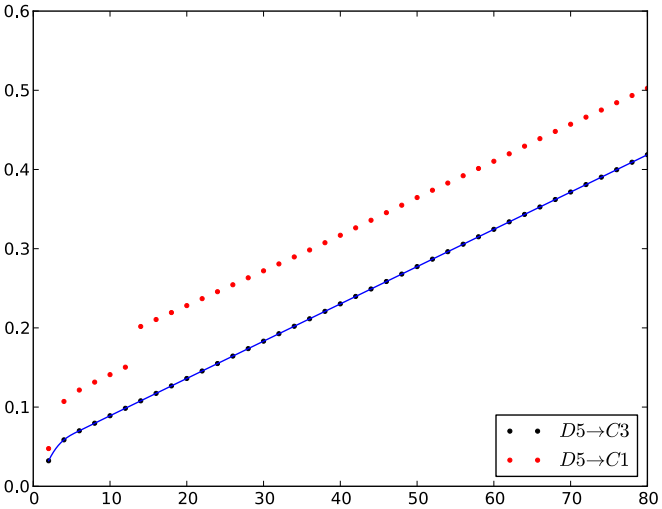

FIG. 8. (Color online) A typical situation at $G_s/G_0 = 5.56$, where the transition via the long instanton turns unfavorable following that of the short instanton. The activation barrier of the long instanton (red dots) increases with L as well as the lifetime so that the wire becomes more and more stable against thinning. The transition direction switches accordingly from thinning to growth.

from short wires, as it would cost excessive bending energy in forming the necessary critical droplet. This conclusion is consistent with Fig. 6, in which the flat barrier of the long instanton disappears at small L.

As the wire is compressed and its cross section continues to grow, the energy of even $C1$ starts to shift upward and eventually it becomes the upper well relative to $D5$; the probability of thinning thereafter decreases (see Fig. 8). A similar analysis can be applied to $D9$, where the role of $C3$ is replaced by $D8$ and $C1$ by $C6$. The transition patterns of $D5$ and $D9$ are sketched in Figs. 9(a) and 9(b).

In Fig. 7, we denote the direction from the upper well to the lower one as the "forward" transition and the reverse as "backward.' With its activation barrier reaching a plateau as $L \to \infty$, the forward transition should occur more frequently than the backward one; we therefore refer to it as the *transition direction*. We emphasize that the terms "forward" and "backward" are defined relative to the upper well, that is, the higher-energy metastable state.

In experiments, the wire is constantly subject to breakup and re-formation. Under elongation, the cross section typically samples all possible stable values before breakup. In reforming the nanowire, on the other hand, there is typically a jump to contact, and not all structures are clearly resolved in the conductance histogram. The relevant lifetime determining whether a given metastable structure is observed experimentally is therefore that governing the thinning process when the nanowire is under tension.

In the following sections, we calculate and display the lifetimes of the $D5$ and $D9$ structures for gold and sodium nanowires.

A. Gold nanowires

In this section, we discuss our results for the stability of the $D5$ and $D9$ structures for gold nanowires.

For $D5$, $G_s/G_0 = 5.56$ corresponds to the critical cross section beyond which the long instanton plays a part in the determination of the lifetime. As the wire becomes thicker, the energy of the long instanton, and therefore the lifetime, increases monotonically. Eventually, the transition $D5 \to C1$, occurring via the long instanton, becomes backward, essentially halting the thinning process. The evolution of the barrier for thinning is plotted in Fig. 10; the energy of the long instanton ranges up to $\Delta E_\infty = 1000$ meV, corresponding to a lifetime $\tau \approx 10^7$ s at $T = 300$ K.

If one considers growth processes, the lifetime may be much shorter. The lifetime of the $D5 \to C6$ process, for example, where $C6$ is a cylindrical state with a higher conductance value, is only of order 10^{-12} s. However, in experimental situations in which tensile stresses bias the system toward thinning, $D5$ should live long enough to be observed experimentally. Atoms can always leave the wire by diffusing out onto the surface of the bulk electrodes, while atoms incorporated into the bulk electrodes cannot readily migrate into the wire, so that thickening may only be possible on reasonable time scales under compression.

For the $D9$ structure, the analysis is similar to that for $D5$, except that the critical cross section for the onset of the long instanton is approximately $G_s/G_0 = 9.3$. Below this value, the

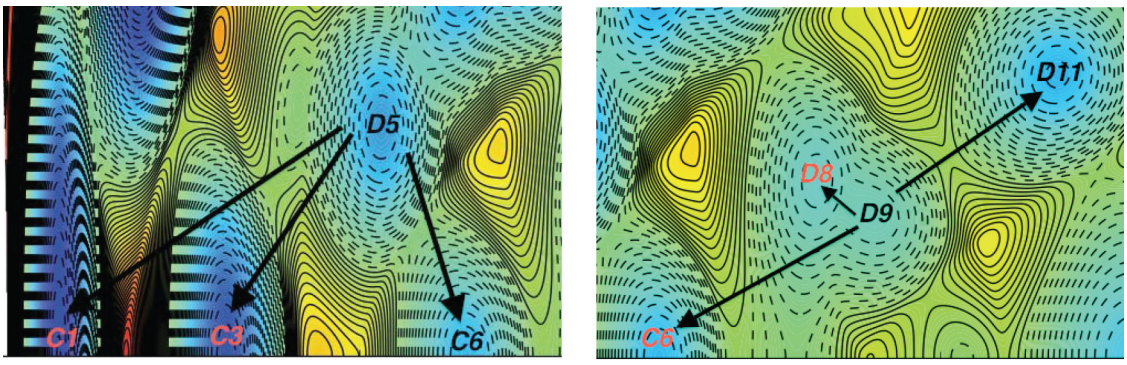

(a) Transition pattern of $D5$ (b) Transition pattern of $D9$

FIG. 9. (Color online) Transition patterns for the structures $D5$ and $D9$. Both thinning and growth are drawn, where the final states of thinning are highlighted in red. Note that for growth only the nearest final state ($C6$ for $D5$ and $D11$ for $D9$) is shown for discussion purposes.

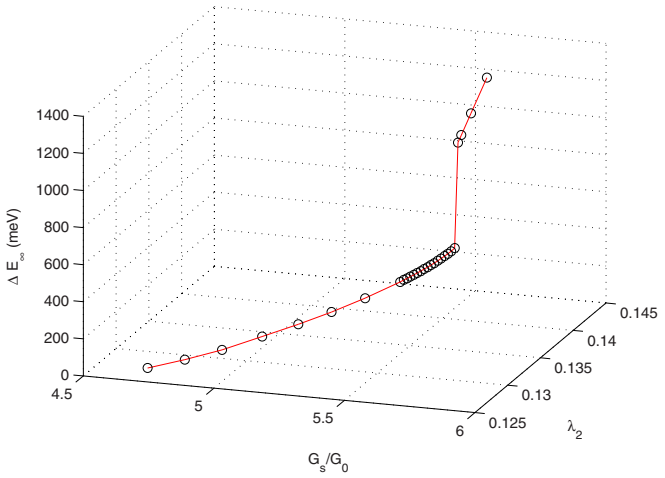

FIG. 10. (Color online) Activation barrier for thinning of the $D5$ structure in Au. The G_s/G_0 axis is related by the Sharvin formula to the continuous variation of the cross section resulting from the change of tensile force; the λ_2 axis is the corresponding variation in the degree of axial symmetry breaking. Below the critical cross section at $G_s/G_0 = 5.56$, the activation barrier ΔE_∞ is determined by the transition $D5 \rightarrow C3$ via the short instanton, while for $G_s/G_0 > 5.56$ the activation barrier is determined by the transition $D5 \rightarrow C1$ (long instanton). The curve stops at the point where the energy of the long instanton becomes unbounded and thinning thus surrenders to growth.

likeliest transition is from $D9$ to $D8$ via the short instanton; above this value, the transition will be from $D9$ to $C6$ via the long instanton. For thicker wires, $D9$ could transition to $D11$ rapidly, with a lifetime of the order of a millisecond. Overall, $D9$ is quite stable against thinning, with a lifetime (determined by the long instanton) of 10^3 s at $T = 100$ K.

B. Sodium nanowires

The qualitative features of the stability of sodium nanowires are similar to those of gold nanowires. However, lifetimes are significantly shorter (cf. Ref. [12]) because of sodium's smaller surface energy.

Nevertheless, $D5$ is quite stable against thinning, with a lifetime of 0.3 ms at $T = 100$ K. The critical cross section above which the long instanton becomes relevant is $G_s/G_0 = 5.48$. $D9$ has a lifetime of 0.057 s at $T = 60$ K or 0.000 12 s at $T = 80$ K. The critical cross section for $D9$ is $G_s/G_0 = 9.3$. Both plateaus are unstable at room temperature, and the same issues concerning growth vs thinning apply to sodium as for gold.

V. DISCUSSION

The previous section discusses a mechanism—the interplay of transitions via short vs long instantons—that is likely to play an important role in determining lifetimes of nonaxisymmetric wires. Physically, this interplay reflects the competition between classical and quantum effects (the latter encapsulated within the electron-shell potential). In the classical regime, a long wire requires a large cross section to stabilize against the Rayleigh instability. However, when quantum effects are taken into account, the deep minima of the electron-shell potential favor thinner structures, giving rise to "magic radii." When quantum effects dominate, the thinning process is favored and the transition from thicker to thinner is forward; when classical effects dominate, the thinning transition becomes backward and hence less favorable. As the cross section is continuously varied from larger to smaller, we find that thinning is inhibited when the initial structure is thicker; the converse is true when it is thinner.

In the purely cylindrical case, thinning and growth reach equilibrium when the wire is at a particular cross-sectional area, as in Fig. 4 of Ref. [12]. The most stable structure and its lifetime can thus be defined at the cusp. In the nonaxisymmetric case, however, there is no similar single point of equilibrium. The rate of growth is generally much faster than that of thinning, so that the wire may escape to a thicker state even if the lifetime for thinning is large. Experimentally, however, $D5$ and $D9$ are observable with lifetimes of the order of milliseconds or larger. We believe this is due to the experimental situation in which applied stresses to the wire inhibit growth. Our model for both thinning and growth implicitly assumes that the transfer of atoms into and out of the wire is instantaneous. This assumption is a reasonable approximation for thinning but not for growth under normal experimental conditions. The observed stability of laboratory nanowires is largely restricted by thinning processes: in experiments the wire usually either thins or breaks up under the pulling force. Given this, our model is quite successful in predicting the stability of $D5$ and $D9$ conductance plateaus against thinning.

ACKNOWLEDGMENTS

The authors are grateful to Seth Merickel for his contributions to the early stages of this work. This work was supported in part by NSF Grant No. PHY-0965015. C.A.S. acknowledges support from the U.S. Department of Energy, Office of Science, under Award No. DE-SC0006699. D.L.S. thanks the John Simon Guggenheim Foundation for a fellowship that partially supported this research.

[1] J. Bürki and C. A. Stafford, Appl. Phys. A **81**, 1519 (2005).
[2] J. Plateau, in *Statique Expérimentale et Théorique des Liquides Soumis aux Seules Forces Moléculaires* (Gautier-Villars, Paris, 1873).
[3] J. Bürki, R. E. Goldstein, and C. A. Stafford, Phys. Rev. Lett. **91**, 254501 (2003).
[4] M. E. T. Molares, A. G. Balogh, T. W. Cornelius, R. Neumann, and C. Trautmann, Appl. Phys. Lett. **85**, 5337 (2004).
[5] A. Bid, A. Bora, and A. K. Raychaudhuri, Proc. SPIE **5843**, 147 (2005).
[6] S. Karim, M. E. Toimil-Molares, A. G. Balogh, W. Ensinger, T. W. Cornelius, E. U. Khan, and R. Neumann, Nanotechnology **17**, 5954 (2006).

[7] A. I. Yanson, I. K. Yanson, and J. M. van Ruitenbeek, Nature (London) **400**, 144 (1999).

[8] A. I. Yanson, I. K. Yanson, and J. M. van Ruitenbeek, Phys. Rev. Lett. **84**, 5832 (2000).

[9] D. F. Urban, J. Bürki, C.-H. Zhang, C. A. Stafford, and H. Grabert, Phys. Rev. Lett. **93**, 186403 (2004).

[10] D. Urban, J. Bürki, A. Yanson, I. Yanson, C. Stafford, J. van Ruitenbeek, and H. Grabert, Solid State Commun. **131**, 609 (2004).

[11] D. F. Urban, J. Bürki, C. A. Stafford, and H. Grabert, Phys. Rev. B **74**, 245414 (2006).

[12] J. Bürki, C. A. Stafford, and D. L. Stein, Phys. Rev. Lett. **95**, 090601 (2005).

[13] J. Bürki, C. A. Stafford, and D. L. Stein, in *Noise in Complex Systems and Stochastic Dynamics II*, edited by Z. Gingl, J. M. Sancho, L. Schimansky-Geier, and J. Kertesz, SPIE Proceedings Series Vol. 5471 (SPIE, Bellingham, WA, 2004), pp. 367–379.

[14] A. I. Mares, D. F. Urban, J. Bürki, H. Grabert, C. A. Stafford, and J. M. van Ruitenbeek, Nanotechnology **18**, 265403 (2007).

[15] L. Gong and D. L. Stein, J. Phys. A: Math. Theor. **43**, 405004 (2010).

[16] L. Gong and D. L. Stein, Phys. Rev. E **84**, 031119 (2011).

[17] S.-G. Ihn and J.-I. Song, Appl. Phys. Lett. **89**, 053106 (2006).

[18] O. V. Astafiev, L. B. Ioffe, S. Kafanov, Y. A. Pashkin, K. Y. Arutyunov, D. Shahar, O. Cohen, and J. S. Tsai, Nature (London) **484**, 355 (2012).

[19] H. Schmid, K. Moselund, M. Bjork, M. Richter, H. Ghoneim, C. Bessire, and H. Riel, in *69th Annual Device Research Conference (DRC)* (IEEE, Santa Barbara, CA, 2011), pp. 181–182.

[20] N. Agraït, A. Levy Yeyati, and J. M. van Ruitenbeek, Phys. Rep. **377**, 81 (2003), and references therein.

[21] N. Agraït, J. G. Rodrigo, and S. Vieira, Phys. Rev. B **47**, 12345 (1993).

[22] C. J. Muller, J. M. van Ruitenbeek, and L. J. de Jongh, Physica C **191**, 485 (1992).

[23] C. J. Muller, J. M. van Ruitenbeek, and L. J. de Jongh, Phys. Rev. Lett. **69**, 140 (1992).

[24] L. Olesen, E. Laegsgaard, I. Stensgaard, F. Besenbacher, J. Schiotz, P. Stoltze, K. W. Jacobsen, and J. K. Norskov, Phys. Rev. Lett. **74**, 2147 (1995).

[25] J. L. Costa-Krämer, N. García, and H. Olin, Phys. Rev. B **55**, 12910 (1997).

[26] H. Ohnishi, Y. Kondo, and K. Takayanagi, Nature (London) **395**, 780 (1998).

[27] C. H. Zhang, F. Kassubek, and C. A. Stafford, Phys. Rev. B **68**, 165414 (2003).

[28] C. A. Stafford, F. Kassubek, J. Bürki, and H. Grabert, Phys. Rev. Lett. **83**, 4836 (1999).

[29] C. A. Stafford, D. Baeriswyl, and J. Bürki, Phys. Rev. Lett. **79**, 2863 (1997).

[30] J. M. van Ruitenbeek, M. H. Devoret, D. Esteve, and C. Urbina, Phys. Rev. B **56**, 12566 (1997).

[31] F. Kassubek, C. A. Stafford, H. Grabert, and R. E. Goldstein, Nonlinearity **14**, 167 (2001).

[32] D. F. Urban and H. Grabert, Phys. Rev. Lett. **91**, 256803 (2003).

[33] D. F. Urban, C. A. Stafford, and H. Grabert, Phys. Rev. B **75**, 205428 (2007).

[34] P. Hänggi, P. Talkner, and M. Borkovec, Rev. Mod. Phys. **62**, 251 (1990).

[35] M. I. Freidlin and A. D. Wentzell, *Random Perturbations of Dynamical Systems* (Springer-Verlag, New York, 1984).

[36] R. S. Maier and D. L. Stein, Phys. Rev. E **48**, 931 (1993).

[37] M. Marder, Phys. Rev. E **54**, 3442 (1996).

[38] Weinan E, W. Ren, and E. Vanden-Eijnden, Phys. Rev. B **66**, 052301 (2002).

[39] Weinan E, W. Ren, and E. Vanden-Eijnden, J. Chem. Phys. **126**, 164103 (2007).

[40] M. Brack, Rev. Mod. Phys. **65**, 677 (1993).

[41] D. F. Urban, J. Bürki, C. A. Stafford, and H. Grabert, *The Nanoscale Free-Electron Model* (CRC Press, Boca Raton, FL, 2010), Vol. 1.

[42] F. Kassubek, C. A. Stafford, and H. Grabert, Phys. Rev. B **59**, 7560 (1999).

[43] M. Brack and R. K. Bhaduri, *Semiclassical Physics*, Frontiers in Physics Vol. 96 (Addison-Wesley, Reading, MA, 1997).